ENVIRONMENTAL RESEARCH
LETTERS

LETTER • OPEN ACCESS

# Satellite-observed SST and chlorophyll reveal contrasting dynamical-biological effects of mesoscale eddies in the North Atlantic

To cite this article: Guiyan Han *et al* 2024 *Environ. Res. Lett.* **19** 104035

IOP Publishing Environ. Res. Lett. 19 (2024) 104035 https://doi.org/10.1088/1748-9326/ad7049

ENVIRONMENTAL RESEARCH
LETTERS



OPEN ACCESS

RECEIVED
27 February 2024

REVISED
12 August 2024

ACCEPTED FOR PUBLICATION
16 August 2024

PUBLISHED
5 September 2024



LETTER

# Satellite-observed SST and chlorophyll reveal contrasting dynamical-biological effects of mesoscale eddies in the North Atlantic

**Guiyan Han**[1,2,3], **Graham D Quartly**[3,*], **Ge Chen**[2,4] and **Jie Yang**[2,4]

[1] Institute of Marine Science and Technology, Shandong University, Qingdao 266237, People's Republic of China
[2] Frontiers Science Centre for Deep Ocean Multispheres and Earth System, School of Marine Technology, Ocean University of China, Qingdao 266100, People's Republic of China
[3] Plymouth Marine Laboratory, Prospect Place, The Hoe, Plymouth PL1 3DH, Devon, United Kingdom
[4] Laboratory for Regional Oceanography and Numerical Modeling, Laoshan Laboratory, Qingdao 266237, People's Republic of China
[*] Author to whom any correspondence should be addressed.

**E-mail:** gqu@pml.ac.uk

**Keywords:** mesoscale eddies, chlorophyll, sea surface temperature, eddy mechanisms, North Atlantic, mixed layer depth

Supplementary material for this article is available online

## Abstract

The influence of mesoscale eddies on chlorophyll (Chl) has received significant attention due to Chl being a proxy for phytoplankton, which plays a crucial role in marine ecosystems. Solely relying on the analysis of satellite-observed Chl poses challenges in determining the phytoplankton response to mesoscale eddies. To address this, our study takes a collaborative approach, utilizing satellite-derived sea surface temperature anomalies (SSTA) and chlorophyll anomalies (CHLA) to comprehensively investigate the dynamical-biological processes associated with eddies in the subtropical and mid-latitude North Atlantic. In the subtropics, the patterns in CHLA and SSTA predominantly exhibit a dipole nature, with the dipole component providing more than 70% of the explained variance (EV). This suggests that eddy stirring is the dominant mechanism driving the observed anomaly patterns. Conversely, in the mid-latitudes, the monopole components ($T_M$) explain more than 60% of the EV, implying a more influential role for eddy trapping and vertical modulations. The signs of the $T_M$ of eddy SSTA persist throughout their lifetime, being consistent with the lowering (raising) of isopycnals within AEs (CEs). However, the subtropical CHLA response is higher in AEs than CEs, indicating additional factors, such as eddy-induced Ekman pumping and/or mixing to a deeper level may be important. This finding is also corroborated by subsurface observations from Argo floats. At mid-latitudes, there is a clear inverse correspondence between the CHLA and mixed layer depth. In contrast, no significant correlation is observed in the subtropics, except during winter when a positive relationship emerges. These patterns suggest that phytoplankton exhibit highly diverse responses to the physical dynamics associated with eddies. Our work offers a method to estimate eddy dynamical-biological impacts on phytoplankton using satellite products, compensating for the limitations of in-situ observations. It also reveals potential contributions to marine primary production, global carbon cycles, and the development of biogeochemical models.

## 1. Introduction

Mesoscale eddies in the ocean are rotating water bodies with diameters of the order of 100 km and lifetimes ranging from days to several years. They have been widely found to transport substances such as water, heat and salt [1–3], while also playing a crucial role in regulating air-sea interactions [4, 5]. Additionally, mesoscale eddies can affect phytoplankton growth by modulating nutrients and light availability [6, 7]. Consequently, they impact primary production and, by extension, the behaviours of zooplankton and

higher trophic predators [8–13], highlighting their significant roles in the marine ecosystem and biogeochemical cycling.

The satellite-derived chlorophyll (Chl) concentration is widely used as a proxy for phytoplankton biomass in the global ocean [14, 15]. Numerous studies have shown higher Chl associated with cyclonic eddies (CEs) than anticyclonic eddies (AEs) [9, 16, 17]. Oppositely, AEs were observed with enhanced Chl concentration in the subtropical oceans [2, 16, 18–20], as well as the Southern Ocean [21–23]. This phenomenon has been widely discussed, whether it is due to eddy modulation stimulating phytoplankton growth [19, 20, 24] or phytoplankton increasing their intracellular pigments in response to dynamic modulations [18, 25], so-called photoacclimation. The former can either be caused by eddy-induced upwelling or deeper mixing that increases nutrient levels, while the latter results from eddy downwelling, which decreases light availability. Based on a numerical model, Dufois *et al* revealed that deeper mixing of winter AEs facility nutrients in the upper ocean, thus leading AEs to be more productive than CEs [19]. Gaube *et al* pointed out that the eddy-induced Ekman upwelling is partly responsible for sustaining positive Chl anomalies in AEs of the South Indian Ocean [20]. Rohr *et al* pointed out that iron availability is elevated in AEs of Southern Ocean, both due to their eddy-induced Ekman pumping and deeper mixing [26]. Conversely, He *et al* explained the enhanced Chl in subtropical AEs by photoacclimation to the low-light environment caused by deeper mixing [18].

The complexity of eddy mechanisms poses challenges in exploring their influences on phytoplankton, solely through satellite-observed Chl. In such cases, sea surface temperature (SST) serves as a dynamic tracer, offering signals modulated by eddy mechanisms. SST has been utilized for identifying normal/abnormal mesoscale eddies [27–29], estimating eddy heat transportation [30, 31], and exploring eddy air-sea interactions [4, 32], suggesting their close connection with eddy dynamics. Joint observations of SST and Chl have been employed to establish multi-observation eddy datasets and multi-parameter index for eddy tracking [33, 34]. They have also been applied to investigate shelf-open sea exchange in individual eddies [35]. Dawson *et al* discussed the seasonal and geographical variabilities in the eddy-induced physical and biological characteristics, focusing exclusively on the Southern Ocean [23]. To the best of our knowledge, there are few studies applying collaborative observations of surface Chl and SST to explore eddy dynamics and their associated phytoplankton response. This approach provides insight into exploring and modeling the impact of eddies in marine ecosystems.

Mesoscale eddies can influence the marine environment via horizontal and vertical dynamical mechanisms (figure S2). Horizontally, (1) eddies stir surface Chl through azimuthal advection, leading to dipole patterns of chlorophyll anomalies (CHLA) and sea surface temperature anomalies (SSTA) along the eddy peripheries [36, 37]. (2) Eddies trap surface heat, Chl and nutrients during their formation, and maintain them over their lifetime, making the SSTA and CHLA monopoles [16, 38]. Vertically, (3) CEs induce upwelling, causing positive CHLA and negative SSTA signals. In contrast, AEs cause downwelling, a mechanism known as eddy pumping [8, 9], which only functions during eddy formation and intensification. (4) The relative motion between surface air and currents generates sustained Ekman upwelling and downwelling in the cores of AEs and CEs throughout their lifetimes, known as eddy-induced Ekman pumping [39, 40]. This mechanism can induce surface signals opposite to eddy pumping, with negative CHLA and positive SSTA within CEs. It slowly attenuates the eddy but coexists with the upwelling/downwelling induced by eddy pumping. (5) Eddies can modulate the mixed layer depths (MLD) by deforming isopycnals, which in turn influences the availability of light and nutrients for phytoplankton growth [41]. This modulation can be driven by eddy pumping and sustained by the rotating eddies, resulting in deeper MLD within AEs and shallower MLDs within CEs. From a biological perspective, eddy-induced upward motion transports nutrients into the euphotic zone and increases light availability, thereby promoting phytoplankton growth. Conversely, eddy-induced downward motion can inhibit phytoplankton growth by reducing nutrient and light levels. However, in oligotrophic regions, the enhanced mixing associated with downwelling can elevate nutrient concentrations within the mixed layer, thereby stimulating phytoplankton growth.

Our study primarily analyzes the collaborative signals of eddy-affected SST and Chl to investigate eddy dynamical-biological mechanisms, with a focus on the North Atlantic Ocean. The region is ideal for marine biological studies, benefiting from the accumulated Argo floats and the zooplankton observations of the Continuous Plankton Recorder project, which are used in a subsequent paper addressing eddies' effect on zooplankton. The North Atlantic is also one of the regions most affected by ocean warming [42]. Clarifying its eddy dynamical-biological processes is of fundamental importance for future marine ecosystem investigations.

## 2. Data and method

Section 2 provides details about the satellite data and Argo floats used in this study, as well as the data

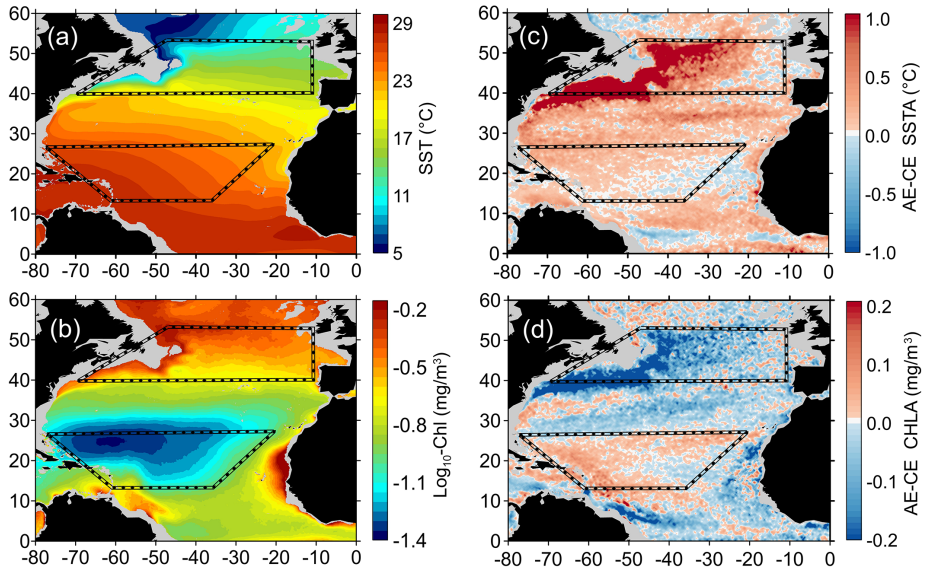


**Figure 1.** Geographical distribution of satellite-observed SST and log-Chl characteristics in the North Atlantic from 01/01/1998 to 31/12/2018. Panels (a) and (b) represent the climatology of SST and Chl, respectively. Panels (c) and (d) show SSTA and CHLA of AEs minus CEs, based on observations within eddy boundaries. The processing of SSTA and CHLA is detailed in section 2.3.2.

processing and analyzing methods. A sketch map illustrating the major steps of the data processing is presented in figure S3.

### 2.1. Study area definition

The distribution of SST in the North Atlantic decreases with increased latitude, displaying a primary gradient direction from northeast to southwest (figure 1(a)). The Chl in the North Atlantic is characterized by a circulatory pattern, with low concentrations in the centre of the subtropical gyre (figure 1(b)). Relatively, the mid-latitude surface is marked by high Chl levels, with phytoplankton growth in the deeper waters being controlled by the availability of sunlight [43].

To explore the eddy dynamical and biological influences, we focus on two sub-regions of the North Atlantic according to eddy-induced SSTA and CHLA. Figures 1(c) and (d) show SSTA and CHLA derived from AEs minus CEs. We identify two broad regions (shown by black lines) for analysis and comparison. The mid-latitude region (from 40° N to 55° N) has high eddy kinetic energy (EKE) and contains Gulf Stream eddies and the North Atlantic Current, and it is well-mixed in winter. In contrast, the subtropical region (from 12° N to 28° N) is relatively quiescent and permanently stratified with a deep Chl maximum [44].

### 2.2. Eddy tracking, identifying and matching with observations

The sea level anomaly (SLA) data utilized in this study are derived from multiple altimeter missions including TOPEX/Poseidon, ERS-1/2, Envisat, Jason-1/2/3, Sentinel-3A, HY-2A, Saral/AltiKa, Cryosat2, and GFO, as released by AVISO [45]. The daily 'all-satellite' SLA dataset is provided on a 0.25° longitude × latitude grid, making full use of all the available altimeters while also providing additional information. To align with Chl products, the all-satellite SLA from 01/01/1998 to 31/12/2018 were employed to produce the eddy dataset. The AVISO two-satellite product is based solely on missions flying on the 10 d and 35 d (or 27 d) sampling patterns (see figure 1 of Quartly *et al* [46]) to provide homogeneous spatial coverage throughout the analysis period, and is utilized to verify the consistency of the 'all-satellite' eddy tracking.

Based on the improved eddy identifying and tracking methods developed by Tian *et al* [47], an eddy dataset of the North Atlantic has been created. For the eddy identification, a high-pass filter was initially applied to global SLA data using a half-power Gaussian filter to effectively identify eddy seed points, which are local maxima or minima. Subsequently, SLA contours were computed at 0.25 cm intervals. The closed SLA contour with the maximum average geostrophic current speed was defined as the eddy boundary and was required to contain no more than one eddy seed. When tracking was performed, for each eddy identified on Day-1, eddies from the next day occurring within a radius of 0.5° from the Day-1 eddy centroid were considered. If multiple Day-2 eddies fall into the search range, the target eddy was determined based on a set of similarity parameters, including kinetic energy, distance, amplitude, and area of the eddy.

To mitigate imperfections in the detection and tracking procedure and ensure the eddy qualities, only robust eddies with lifetimes longer than 30 d

were retained for further analysis [48]. The apparently low occurrence of eddies in the Gulf Stream is due to the fact that most of its eddies have lifetimes shorter than 30 d (figure 6(c) of Chen and Han [49]). Additionally, eddy boundaries were required to include more than 8 SLA grid points, with amplitudes larger than 1 cm and water depths deeper than 1000 m.

The selected mesoscale eddies were matched with in-situ or gridded observations. The relative radius ($Rr$) of each observation associated with an eddy snapshot ranges from 0 when it coincides with the eddy centroid to 2 when it is twice the irregular eddy boundary. The azimuth ($\theta$) from the eddy-centroid to the observation direction was also calculated. Therefore, the position of an observation relative to an eddy snapshot can be described by its polar coordinates ($Rr$, $\theta$).

### 2.3. Satellite products and composite analyzes

#### 2.3.1. Satellite data

The multi-satellite merged Chl product from 01/01/1998 to 31/12/2018 was generated by Plymouth Marine Laboratory as a part of the Ocean Colour CCI programme [50], funded by the European Space Agency. We utilized v5.0 data, which comprise daily composites from merged sensor products (MERIS, MODIS-Aqua, SeaWiFS, VIIRS) with a spatial resolution of 4 km.

The 0.25° daily optimally interpolated sea surface temperature (OI-SST) product version 2.0, utilizing AVHRR, is distributed by NOAA Physical Sciences Laboratory to provide SST from 01/01/1998 to 31/12/2018. It has been employed to explore dynamic effects related to eddies near the ocean surface.

#### 2.3.2. Data anomalies

To mitigate the impact of gaps resulting from clouds and short-term variability, satellite observations of Chl and SST were subject to temporal and spatial filtering. This process also discerns the Chl response to eddies in comparison to water areas outside the eddies. Anomalies in Chl and SST were subsequently derived through the following methods:

(1) The Chl observations were fitted on a 0.25° × 0.25° grid and base 10 logarithm-transformed (log-Chl) due to their tendency to exhibit a log-normal distribution [36, 51].
(2) The Chl and SST time series for each location was running averaged with an 18 d window to attenuate variability shorter than 30 d [36]. The adoption of an 18 d window size proved to be effective in minimizing data gaps (see details in Supporting Information text S1). Following Chelton *et al* [36], the time series were then high-pass filtered to attenuate variability with periods longer than 400 d (1 yr and 1 month).
(3) The time-filtered fields underwent additional spatial processing, specifically a high-pass filter removing wavelength scale larger than 6° × 6° (longitude × latitude). This procedure was applied to generate anomaly fields. The generated anomalies of log-Chl will be referred to as CHLA, and anomalies of SST will be referred to as SSTA in subsequent discussions.

#### 2.3.3. Eddy-centric composite analyses

Observations within two times eddy boundaries are composited to show eddy-affected spatial patterns. The eddy-centric composite analyses, based on spatially filtered fields, involve the following steps:

(1) For each daily eddy snapshot, a standard array with 21 rows and 21 columns was established. The centre of the standard array represents the eddy centroid, and the polar coordinates ($Rr$, $\theta$) of each grid can be determined:

$$Rr(i,j) = \frac{\mathrm{ER}\{(i,j),(i_0,j_0)\}}{10}\ (i,j = 0,1,2\ldots20) \tag{1}$$

$$\theta = Az\{(i,j),(i_0,j_0)\}\ (i,j = 0,1,2\ldots20) \tag{2}$$

where $i_0 = 10$, $j_0 = 10$. $ER$ represents Euclidean distance, and $Az$ represents the azimuth coordinate from ($i_0$, $j_0$) to ($i$, $j$).
(2) The observations within two times eddy boundaries were assigned to standard arrays according to polar coordinates ($Rr$, $\theta$). Those points within $Rr = 2$ had a 3 × 3 moving average filter applied to reduce gaps.
(3) For eddy composites, all eddy snapshots were aligned within a translating and rotating frame of reference, determined by the orientation of the large-scale Chl or SST gradient. The large-scale fields were defined as 14 times the eddy radii from the monthly climatology. The ambient gradient vector was rotated to align the large-scale gradient vector from south to north.
(4) The standard arrays were aggregated and averaged according to eddy polarity, regions, months, EKE, and other relevant factors to generate the final composite results.

#### 2.3.4. Decomposition of CHLA/SSTA composites

To analyze the influence of various eddy mechanisms on SSTA and CHLA, their composites were decomposed into dipole ($T_D$) and monopole ($T_M$) components. Following the approach outlined by [21, 52], the $T_M$ of the eddy composites were derived by averaging composites ($T_C$):

$$T_M(Rr) = \overline{T_C(Rr)} \tag{3}$$

where $Rr$ represents radial coordinate ranging from 0 to 2. Then, the $T_D$ of SSTA/CHLA can be obtained:

$$T_D(Rr,\theta) = T_C(Rr,\theta) - T_M(Rr,\theta). \quad (4)$$

*2.3.5. The structure index and explained variance*

The structure index ($\alpha$) used by Lv *et al* [5] is introduced to evaluate pattern similarities between eddy composites and their components. The index $\alpha_M$ and $\alpha_D$ of the monopole and $T_D$ are defined by:

$$\alpha_M = \mathrm{PC}(T_M(Rr,\theta), T_C(Rr,\theta)) \quad (5a)$$

$$\alpha_D = \mathrm{PC}(T_D(Rr,\theta), T_C(Rr,\theta)) \quad (5b)$$

where $PC$ indicates the calculation of the Pearson correlation coefficient; $T_C$ indicates the composite field; $T_D$ and $T_M$ represent the dipole and $T_M$ of $T_C$; $(Rr, \theta)$ represents polar coordinates of $T_C$, $T_M$ and $T_D$, with $Rr$ ranging from 0 to 2. Besides structure index $\alpha$, the explained variance (EV) indicator is introduced to quantify the contributions of $T_M$ and $T_D$ to the eddy composites [21]. For $T_M$, the EV is defined:

$$\lambda = \frac{\sum_{i=1}^{n}(x_i-\mu)^2}{n} \quad (6)$$

$$\mathrm{EV} = \frac{\lambda_M}{\lambda_M+\lambda_D} \times 100\%. \quad (7)$$

Equation (6) calculates the variance $\lambda$, where $x$ represents observations, $\mu$ is the expectation, and $n$ indicates the number of observations. In equation (7), $\lambda_M$ and $\lambda_D$ indicate the variance of $T_M$ and $T_D$ respectively.

### 2.4. Core Argo data and processing

The Argo project is responsible for the deployment of thousands of autonomous profiling floats in the global ocean. Within the Core Argo program, floats return sea temperature (ST) and salinity profiles from the surface to a depth of 2000 m every 10 d. The program has successfully reached and maintained the target of 3000 operating floats since late 2007.

When processing temperature profiles, a moving median filter (with a window size of 5) was employed to eliminate noisy spikes. The profiles were subsequently linearly interpolated with a vertical resolution of 5 m. Then, the ST profiles are aggregated monthly onto a 2° × 2° grid to generate local mean profiles, The sea temperature anomalies for each profile were derived by referencing these mean profiles.

Holte *et al* [53] produced a database of MLD derived from Argo floats; in our analysis, we use the MLD calculated according to a density threshold relative to surface waters. The MLD dataset is well-sampled, comprising 62 122 observations collected within eddies from 1998 to 2018. To derive MLD anomalies (MLDA), the monthly climatology was subtracted from each 2° × 2° grid cell.

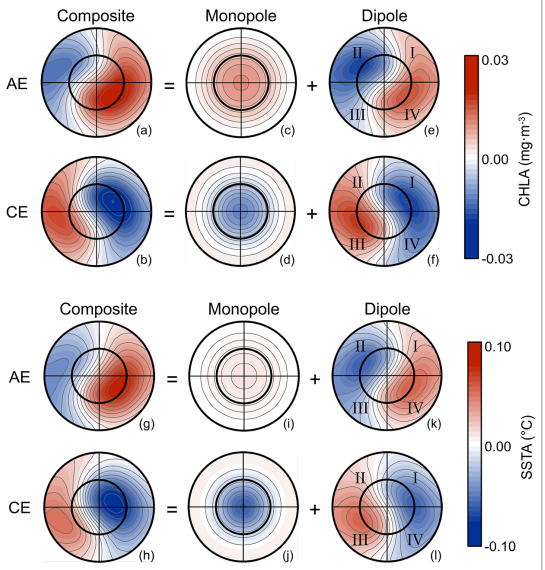


**Figure 2.** The composite of near-surface CHLA (upper rows) and SSTA (lower rows) affected by eddies of the subtropical North Atlantic, for the period 01/01/1998–31/12/2018. The inner and outer circles indicate one and two-times normalized eddy boundaries. The composite patterns are decomposed into monopole and dipole components, and I, II, III and IV indicate quadrants.

## 3. Result and discussion

### 3.1. Composite structures of eddy-induced SSTA and CHLA

Through an analysis of a satellite-derived eddy dataset spanning 21 yr, along with SST and Chl observations, we were able to monitor thousands of eddies in the North Atlantic. The composite patterns of their associated CHLA and SSTA are depicted in figure 2 (subtropical) and figure 3 (mid-latitude) respectively.

The subtropical eddies exhibit dipole patterns both in CHLA and SSTA (figures 2(a), (b), (g) and (h)). In contrast, mid-latitude eddies exhibit shifted monopole patterns (figures 3(a), (b), (g) and (h)). The patterns of these observed composites suggest that they are comprehensively affected by various eddy mechanisms.

The CHLA and SSTA composites were decomposed using the method outlined in section 2.3.4. The $T_M$ and $T_D$ are depicted in the second and third columns for subtropical eddies in figure 2, and for mid-latitude eddies in figure 3. With regard to the polarity of component signals, $T_D$ of CHLA and SSTA exhibit similarities. The negative values of AEs (CEs) are observed in the II (I) quadrants, and positive (negative) poles of AEs (CEs) appear in the IV (III) quadrants. These patterns are determined by directions of background gradients and eddy rotation, with similar effects on surface SST and Chl, consistent with eddy stirring as the dominant process.

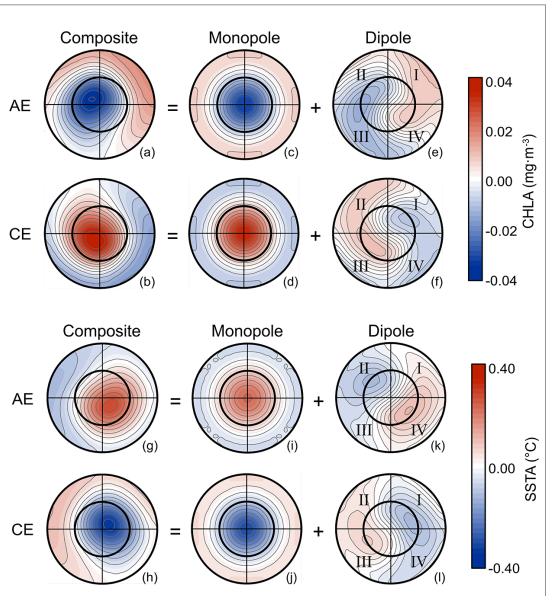


**Figure 3.** Same as figure 2 but for mid-latitude region.

**Table 1.** Structure index ($\alpha$) and explained variance (EV) of CHLA/SSTA composites and components.

| | Eddy polarity | $\alpha_M$ | $\alpha_D$ | $EV_M$ (%) | $EV_D$ (%) |
|---|---|---|---|---|---|
| Sub SSTA | AE | 0.37 | 0.93 | 12 | 88 |
| | CE | 0.52 | 0.88 | 25 | 75 |
| Sub CHLA | AE | 0.34 | 0.94 | 10 | 90 |
| | CE | 0.37 | 0.94 | 12 | 88 |
| Mid SSTA | AE | 0.84 | 0.59 | 67 | 33 |
| | CE | 0.90 | 0.51 | 79 | 21 |
| Mid CHLA | AE | 0.86 | 0.56 | 72 | 28 |
| | CE | 0.91 | 0.48 | 81 | 19 |

Regarding $T_M$, mid-latitude AEs display negative CHLA and positive SSTA, and CEs do the opposite (figures 3(c), (d), (i) and (j)). However, subtropical AEs exhibit positive signals in both CHLA and SSTA components, and CEs show negative ones (figures 2(c), (d), (i) and (j)).

### 3.2. Competition between monopole and dipole components

The $\alpha$ and EV of CHLA and SSTA components were obtained, as presented in table 1. It shows that the $T_D$ of subtropical eddies exhibit much larger $\alpha$ and EV values than monopole ones. This suggests that eddy stirring serves as the dominant mechanism, which may be attributed to the lower intensity of subtropical eddies (table S1). For mid-latitude eddies, their $T_D$ show lower EV and $\alpha$ than monopoles, which is affected by the eddy trapping and eddy vertical perturbations.

Examining the signal variations over the eddy lifetime is an important way to distinguish different mechanisms. For both subtropical and mid-latitude eddies, the average $T_M$ stay largely unchanged during their normalized lifetime, with CHLA/SSTA forming at their initial stage (figure S4). This is similar to the eddy trapping patterns revealed by Gaube *et al* [16]. However, the observed CHLA and SSTA during normalized lifetime deviate from the simulation results obtained using the method of Rohr *et al* [54]. The simulated CHLA exhibit increasing trends and SSTA show decreasing ones, with the magnitude of SSTA much higher than observations both in the subtropics and mid-latitudes (table S2). This indicates that eddy trapping may not be the dominant mechanism in forming monopoles over the eddy lifetime.

### 3.3. Competition between eddy downward and upward motion

Simplistically, it might be expected that the substances trapped by eddies remain constant throughout their lifetime. However, they might be changed due to phytoplankton grazing, air-sea heat exchange, and exchange with their surrounding waters. Furthermore, as eddies migrate across SST and Chl gradients, the external reference values will change. This poses a challenge to remove the monopole component induced by eddy trapping, making it difficult to compare the vertical eddy perturbations.

To focus specifically on the vertical eddy mechanisms, an Argo-derived MLD dataset was analyzed. The monthly MLD associated with AEs and CEs are depicted in figure 4, where the AEs (CEs) exhibit deeper (shallower) MLD than outside eddies. It indicates that the physical differences created by eddies persist throughout the seasonal cycle, where the lowering (raising) of isopycnals in AEs (CEs) may help (hinder) deeper mixing during the winter. Such changes in MLD can affect the availability of nutrients later in the year, especially given the nutrient-limited surface waters of the subtropics.

The CHLA and SSTA variations along with EKE can also indicate vertical eddy dynamics (figure 5). The impacts of mean EKE on anomalies during the eddy initial stage (vertical dashed line in figure 5) are relatively weak. After that, anomalies induced by mid-latitude eddies increase strongly with EKE, while those in subtropical regions show a weak enhancement, which may be related to the difference in eddy intensities between the two regions (table S1).

For the physical tracer SSTA, eddies of various intensities exhibit positive (negative) signals within AEs (CEs) both in mid-latitude and subtropical regions (figures 5(b) and (d)), supporting the conclusion that downward (upward) motion dominates. This conclusion is also supported by subsurface temperature profiles (figure S5), which show enhanced ST anomalies with increasing EKE.

Biological tracers (CHLA) display regional differences, implying various dynamical-biological processes. Negative (positive) anomalies are observed in mid-latitude AEs (CEs), while positive (negative) anomalies are observed in subtropical AEs (CEs) (figures 5(a) and (c)). This may be explained by

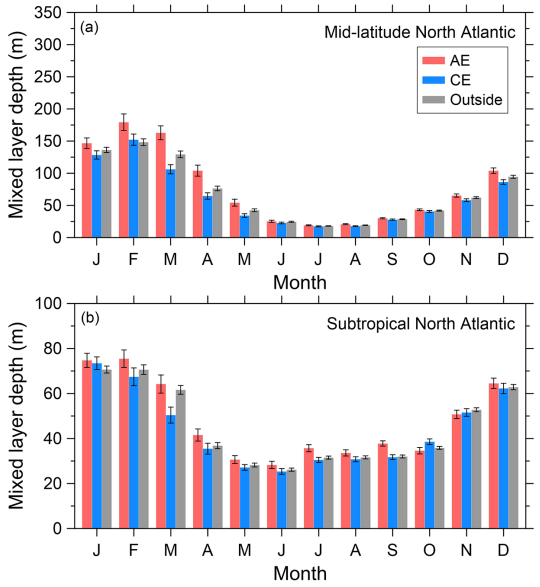


**Figure 4.** Monthly MLD associated with AEs, CEs and outside eddies. The error bars indicate ±2 times the standard error. For AEs and CEs, only data within eddy boundaries ($Rr < 1$) were utilized.

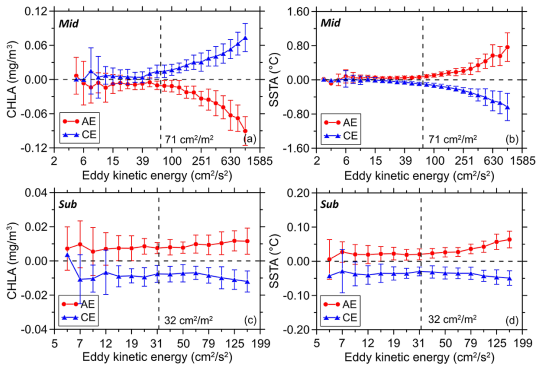


**Figure 5.** Variations of mean CHLA and SSTA in relation to EKE for eddy monopole components. (a) and (b) are for mid-latitude North Atlantic; (c) and (d) are for subtropical North Atlantic. Note the difference in the *x*-axis scale. The error bars indicate ±1 times the standard deviation. The vertical dashed lines and the labels indicate the mean EKE of eddy initial stage (normalized lifetime < 0.05). Only data within eddy boundaries ($Rr < 1$) were utilized.

the upward motion of mid-latitude CEs bringing nutrient-rich water to the euphotic layer, promoting phytoplankton growth. One explanation for the positive CHLA within subtropical AEs is that their mixing (see figure 4) can contribute to phytoplankton photoacclimation, leading to an increase in Chl pigments [18]. Also, some studies have shown that the deeper mixing of AEs during wintertime enhances the nutrients, thereby making AEs more productive than CEs [19]. Meanwhile, some studies have suggested that AEs can persistently induce Ekman upwelling, even though they still retain the positive SSTA [40, 55]. The biological significance of this process warrants further investigation by considering the light level, the nutrient availability and the dynamics of Ekman velocity.

### 3.4. Seasonal implications of eddy dynamical-biological effects

Investigating the seasonal variations of eddy-induced CHLA and SSTA will ensure a comprehensive understanding of seasonal eddy dynamics. The monthly averaged $T_M$ generally exhibit all-season positive (negative) SSTA within both-region AEs (CEs), negative (positive) CHLA within mid-latitude AEs (CEs), and positive (negative) CHLA within subtropical AEs (CEs) (figure S6). These results for SSTA support the maintenance of the initial lowering (raising) of isopycnals upon formation throughout all seasons, consistent with the results shown in figure 4. As for CHLA, the contrasting results indicate different eddy dynamical-biological processes between mid-latitude and subtropical regions.

The impacts of MLD on the eddy dynamical-biological processes are critically important. Mid-latitude AEs consistently exhibit lower CHLA than CEs from January to December. On one hand, the lowered isopycnals associated with AEs reduce nutrient levels; on the other hand, deeper mixing exacerbates light limitation for phytoplankton, as supported by the decreased differences between AEs and CEs during summer (figure S6). In the subtropical region, the differences in CHLA and SSTA between AEs and CEs are evidently reduced during summer and autumn, when the MLD are relatively shallow. The higher Chl within subtropical AEs is likely due to changes in light availability or nutrient levels caused by deeper mixing.

The modulation of MLD by eddies and their biological impact over the seasonal cycles have been extensively reported in the Southern Ocean [22, 26, 54]. Temporal and spatial variations in the ocean background are crucial in modulating light and nutrient availability of phytoplankton, thereby significantly influencing the diversity of eddy biological effects [26, 54].

Such seasonal features are also observed in the North Atlantic. Figure 6 depicts scatter diagrams of eddy-induced MLDA versus CHLA. For the mid-latitude region, CHLA are significantly negatively correlated with MLDA ($p < 0.05$), especially during summertime. The mid-latitude region is nutrient-rich but light-limited and has a much deeper MLD than the subtropics (especially in winter, see figure S7). Deeper mixing could reduce light availability, thereby limiting phytoplankton growth, similar to findings reported in the Southern Ocean [26].

However, the subtropical region exhibits a positive correlation between CHLA and MLDA during wintertime (figure 6(e), $p < 0.001$), when the mean MLD is deeper than in other seasons (figure S7), allowing greater mixing of nutrients. Therefore, the increased Chl with deeper MLD is likely due

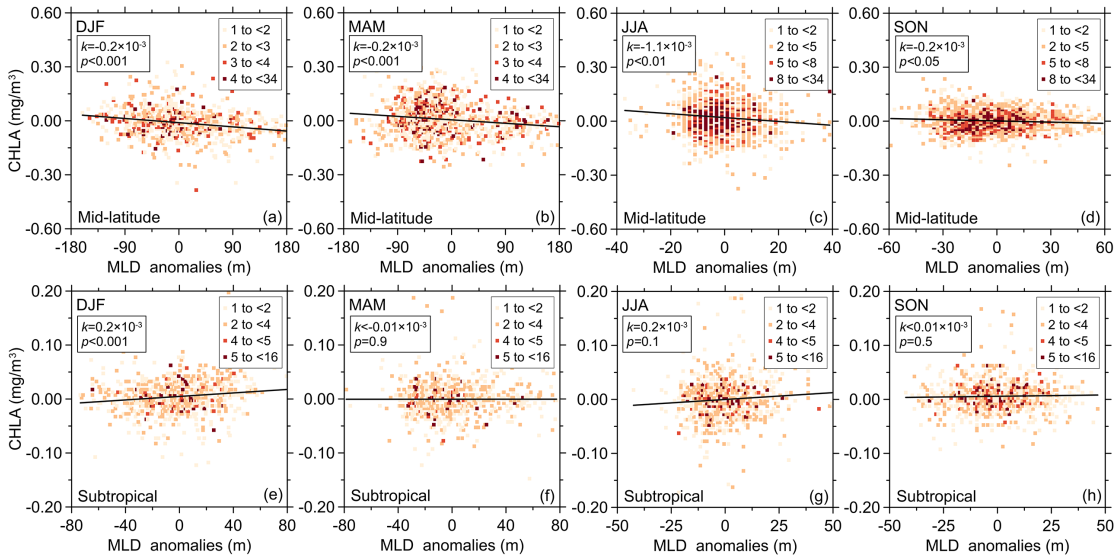


**Figure 6.** Scatter diagrams of eddy-induced MLDA versus CHLA of various seasons. Colors represent the density of observations. The linear fits were overlaid, with $k$ and $p$ representing their slope and significance. DJF, MAM, JJA and SON represent winter, spring, summer and autumn respectively. Only data within boundaries ($Rr < 1$) of AEs and CEs were utilized.

to phytoplankton growth, in agreement with Dufois *et al* [19]. Meanwhile, it can be inferred that during spring, summer, and autumn when MLD values are shallower (figure S7), the higher Chl in AEs compared with CEs may be due to the phytoplankton photoacclimation [18], or increased MLD allowing higher-pigment phytoplankton to reach the surface to be observed by satellites [18]. However, this needs to be further explored considering the effects of eddy-induced Ekman pumping.

## 4. Summary

Eddies provide a critical component in the transport of water, heat, salt and nutrients across the ocean. Vertically, they affect mixing, upwelling/downwelling and isopycnals, with resultant changes in the MLD. Their effects on phytoplankton are complex with often competing mechanisms due to eddy trapping, stirring as well as eddy pumping and Ekman pumping, with effects varying regionally and seasonally. In this paper, we explored the physical and biological data associated with CEs and AEs in two contrasting regions of the North Atlantic. The first region is the mid-latitudes, characterized by a deep mixed layer, nutrient-rich waters, and numerous highly energetic eddies. The second region is the subtropics, noted for less vigorous eddies, oligotrophic waters, and stable stratification throughout the year.

This paper concentrated on the phytoplankton using surface estimates of Chl derived from satellite radiances; a subsequent paper will examine the zooplankton data. Although fluorescence is often used as a proxy for biomass, it should be recalled that a number of factors affect the relationship between fluorescence and Chl, and between Chl and biomass, which are discussed in section 2.4 of Quartly *et al* [44]. Our spatial filtering process i.e. comparing data inside and outside eddies should minimize some of these effects, but short-time physiological responses, such as photoacclimation are an aspect of our results.

Our study primarily explored the dominant eddy mechanisms in the mid-latitude and subtropical North Atlantic, as well as the differences in eddy dynamical-biological processes between the two regions. We conducted a collaborative analysis of satellite SST and Chl observations, treating the eddy-induced SSTA as tracers of eddy dynamics. The composite patterns of CHLA and SSTA were decomposed into $T_M$ and $T_D$ and evaluated as functions of region, time of year and EKE. For the subtropics, the dipole component exhibited the highest EV (figure 2), which is indicative of eddy stirring being the main cause of the anomaly pattern. The monopole component of subtropical eddies was weak and varied little with EKE (figures 5(c) and (d)). In contrast, the monopole component dominated at mid-latitudes (figure 3), and increased substantially with EKE (figures 5(a) and (b)). The polarity of the monopoles agreed with the paradigm of intense downward (upward) modulation of AEs (CEs), but the magnitude showed minimal evolution through the eddy lifetime (figure S4). Surprisingly, in the subtropics, the polarity of the weak CHLA monopole was reversed compared to that at mid-latitudes, even at inception (figure S4(c)), implying that other processes may have contributed to the anomaly signal. Argo data confirmed that AEs generally had deeper MLD than CEs throughout the year for both regions

(figure 4). However, for mid-latitudes, an increase in MLD was significantly correlated with a decrease in CHLA, whereas for the subtropics, a positive correlation was observed in winter, with no correspondence in other seasons (figure 6). A possible interpretation is that at mid-latitudes, the phytoplankton are mixed deeper and get less sunlight when MLD increases, while in the subtropics, an increase in MLD permits access to a larger reservoir of nutrients.

Our work offers a method to estimate eddy dynamics and their biological impacts on phytoplankton using satellite-observed SST and Chl. This approach proved valuable in investigating regional and seasonal eddy effects when subsurface observations are limited. Meanwhile, our findings make certain contributions to the development of global biogeochemical models.

## Data availability statement

For satellite products, the sea level anomalies dataset (1998–2018) distributed by AVISO [45] can be accessed at https://resources.marine.copernicus.eu/products.

The mesoscale eddy dataset (1998–2018) produced by Tian *et al* [47] is public at https://data.casearth.cn/en/sdo/detail/5fa668ad1f4600005e005ba3.

The Ocean Coulour CCI product (1998–2018) is distributed by Plymouth Marine Laboratory [50] at https://climate.esa.int/en/projects/ocean-colour/data/.

Sea surface temperature product (OI SST V2, 1998–2018) distributed by NOAA Physical Sciences Laboratory [56] can be available at: https://psl.noaa.gov/data/gridded/data.noaa.oisst.v2.highres.html.

For Argo floats [57] from 1998 to 2018 can be found at ftp://ftp.ifremer.fr/ifremer/argo.

The mixed layer database using Argo profiles [53] is available at http://mixedlayer.ucsd.edu/.

All data that support the findings of this study are included within the article (and any supplementary files).

## Acknowledgments

This research was jointly supported by the National Natural Science Foundation of China (Grant No. 42030406), the Science and Technology Innovation Project for Laoshan Laboratory (Grant No. LSKJ202204301), and the research time of Graham D. Quartly was supported by project IFADO. We are very grateful to China Scholarship Council for its support for academic visiting of Guiyan Han at Plymouth Marine Laboratory. We extend our gratitude to two anoymous reviewers for their critical insights and valuable comments. We appreciated comments from Liz Atwood and Giorgio Dall'Olmo on a draft version of this paper.

## ORCID iDs

Guiyan Han https://orcid.org/0000-0002-6403-7924
Graham D Quartly https://orcid.org/0000-0001-9132-9511
Ge Chen https://orcid.org/0000-0003-4868-5179
Jie Yang https://orcid.org/0000-0002-4461-1749

## References

[1] Zhang Z G, Wang W and Qiu B 2014 Oceanic mass transport by mesoscale eddies *Science* **345** 322–4
[2] Dong C M, McWilliams J C, Liu Y and Chen D K 2014 Global heat and salt transports by eddy movement *Nat. Commun.* **5** 3294
[3] Nencioli F, Dall'Olmo G and Quartly G D 2018 Agulhas ring transport efficiency from combined satellite altimetry and Argo profiles *J. Geophys. Res.: Oceans* **123** 5874–88
[4] Frenger I, Gruber N, Knutti R and Münnich M 2013 Imprint of Southern Ocean eddies on winds, clouds and rainfall *Nat. Geosci.* **6** 608–12
[5] Lv M K, Wang F, Li Y L, Zhang Z G and Zhu Y N 2022 Structure of sea surface temperature anomaly induced by mesoscale eddies in the North Pacific Ocean *J. Geophys. Res.: Oceans* **127** e2021JC017581
[6] Wang Y, Yang J and Chen G 2023 Euphotic zone depth anomaly in global mesoscale eddies by multi-mission fusion data *Remote Sens.* **15** 1062
[7] McGillicuddy Jr D J and Robinson A R 1997 Eddy-induced nutrient supply and new production in the Sargasso Sea *Deep-Sea Res.* I **44** 1427–50
[8] McGillicuddy Jr D J, Robinson A R, Siegel D A, Jannasch H W, Johnson R, Dickeys T, McNeil J, Michaels A F and Knap A H 1998 Influence of mesoscale eddies on new production in the Sargasso Sea *Nature* **394** 263–6
[9] Falkowski P G, Ziemann D, Kolber Z and Bienfang P K 1991 Role of eddy pumping in enhancing primary production in the ocean *Nature* **352** 55–58
[10] Arostegui M C, Gaube P, Woodworth-Jefcoats P A, Kobayashi D R and Braun C D 2022 Anticyclonic eddies aggregate pelagic predators in a subtropical gyre *Nature* **609** 535–40
[11] Oschlies A and Garcon V 1998 Eddy-induced enhancement of primary production in a model of the north Atlantic Ocean *Nature* **394** 266–9
[12] Xing Q, Yu H, Wang H, Ito S and Yu W 2024 Mesoscale eddies exert inverse latitudinal effects on global industrial squid fisheries *Sci. Total Environ.* **950** 175211
[13] Xing Q W, Yu H Q, Wang H, Ito S I and Chai F 2023 Mesoscale eddies modulate the dynamics of human fishing activities in the global midlatitude ocean *Fish Fisheries* **24** 527–43
[14] Mahadevan A 2014 Eddy effects on biogeochemistry *Nature* **506** 168–9
[15] Longphuirt S N, McDermott G, O'Boyle S, Wilkes R and Stengel D B 2019 Decoupling abundance and biomass of phytoplankton communities under different environmental controls: a new multi-metric index *Front. Mar. Sci.* **6** 312
[16] Gaube P, McGillicuddy Jr D J, Chelton D B, Behrenfeld M J and Strutton P G 2014 Regional variations in the influence of mesoscale eddies on near-surface chlorophyll *J. Geophys. Res.: Oceans* **119** 8195–220
[17] He Q Y, Zhan H G, Cai S Q and Li Z M 2016 Eddy effects on surface chlorophyll in the northern South China Sea: mechanism investigation and temporal variability analysis *Deep-Sea Res.* I **112** 25–36
[18] He Q Y, Zhan H G, Cai S Q and Zhan W K 2021 Eddy-induced near-surface chlorophyll anomalies in the subtropical gyres: biomass or physiology? *Geophys. Res. Lett.* **48** e2020GL091975

[19] Dufois F, Hardman-Mountford N J, Greenwood J, Richardson A J, Feng M and Matear R J 2016 Anticyclonic eddies are more productive than cyclonic eddies in subtropical gyres because of winter mixing *Sci. Adv.* **2** e1600282
[20] Gaube P, Chelton D B, Strutton P G and Behrenfeld M J 2013 Satellite observations of chlorophyll, phytoplankton biomass, and Ekman pumping in nonlinear mesoscale eddies *J. Geophys. Res.: Oceans* **118** 6349–70
[21] Frenger I, Münnich M and Gruber N 2018 Imprint of Southern Ocean mesoscale eddies on chlorophyll *Biogeosciences* **15** 4781–98
[22] Song H, Long M C, Gaube P, Frenger I, Marshall J and McGillicuddy Jr D J 2018 Seasonal variation in the correlation between anomalies of sea level and chlorophyll in the Antarctic Circumpolar Current *Geophys. Res. Lett.* **45** 5011–9
[23] Dawson H R S, Strutton P G and Gaube P 2018 The unusual surface chlorophyll signatures of southern ocean eddies *J. Geophys. Res.: Oceans* **123** 6053–69
[24] He Q Y, Zhan H G, Shuai Y P, Cai S Q, Li Q P, Huang G L and Li J M 2017 Phytoplankton bloom triggered by an anticyclonic eddy: the combined effect of eddy-Ekman pumping and winter mixing *J. Geophys. Res.: Oceans* **122** 4886–901
[25] Cornec M, Laxenaire R, Speich S and Claustre H 2021 Impact of mesoscale eddies on deep chlorophyll maxima *Geophys. Res. Lett.* **48** e2021GL093470
[26] Rohr T, Harrison C, Long M C, Gaube P and Doney S C 2020 Eddy-modified iron, light, and phytoplankton cell division rates in the simulated Southern Ocean *Glob. Biogeochem. Cycle* **34** e2019GB006380
[27] Zhang H F, Huang B X, Chen G, Ge L Y and Radenkovic M 2022 An efficient oceanic eddy identification method with XBT data using transformer *IEEE J. Sel. Top. Appl. Earth Obs. Remote Sens.* **15** 9860–72
[28] Cui W, Yang J G, Jia Y J and Zhang J 2022 Oceanic eddy detection and analysis from satellite-derived SSH and SST fields in the Kuroshio Extension *Remote Sens.* **14** 5776
[29] Liu Y J, Zheng Q A and Li X F 2021 Characteristics of global ocean abnormal mesoscale eddies derived from the fusion of sea surface height and temperature data by deep learning *Geophys. Res. Lett.* **48** e2021GL094772
[30] Qiu B and Chen S M 2005 Eddy-induced heat transport in the subtropical North Pacific from Argo, TMI, and altimetry measurements *J. Phys. Oceanogr.* **35** 458–73
[31] Hausmann U and Czaja A 2012 The observed signature of mesoscale eddies in sea surface temperature and the associated heat transport *Deep-Sea Res.* I **70** 60–72
[32] Aguedjou H M A, Chaigneau A, Dadou I, Morel Y, Baloitcha E and Da-Allada C Y 2023 Imprint of mesoscale eddies on air-sea interaction in the tropical Atlantic Ocean *Remote Sens.* **15** 3087
[33] Dong C M *et al* 2022 The near-global ocean mesoscale eddy atmospheric-oceanic-biological interaction observational dataset *Sci. Data* **9** 436
[34] Roman-Stork H L, Byrne D A and Leuliette E W 2023 MESI: a multiparameter eddy significance index *Earth Space Sci.* **10** e2022EA002583
[35] Shapiro G I, Stanichny S V and Stanychna R R 2010 Anatomy of shelf-deep sea exchanges by a mesoscale eddy in the North West Black Sea as derived from remotely sensed data *Remote Sens. Environ.* **114** 867–75
[36] Chelton D B, Gaube P, Schlax M G, Early J J and Samelson R M 2011 The influence of nonlinear mesoscale eddies on near-surface oceanic chlorophyll *Science* **334** 328–32
[37] Siegel D A, Peterson P, McGillicuddy Jr D J, Maritorena S and Nelson N B 2011 Bio-optical footprints created by mesoscale eddies in the Sargasso Sea *Geophys. Res. Lett.* **38** L13608
[38] Amos C M, Castelao R M and Medeiros P M 2019 Offshore transport of particulate organic carbon in the California current system by mesoscale eddies *Nat. Commun.* **10** 4940
[39] McGillicuddy Jr D J *et al* 2007 Eddy/wind interactions stimulate extraordinary mid-ocean plankton blooms *Science* **316** 1021–6
[40] Gaube P, Chelton D B, Samelson R M, Schlax M G and O'Neill L W 2015 Satellite observations of mesoscale eddy-induced Ekman pumping *J. Phys. Oceanogr.* **45** 104–32
[41] McGillicuddy Jr D J 2016 Mechanisms of physical-biological-biogeochemical interaction at the oceanic mesoscale *Annu. Rev. Mar. Sci.* **8** 125–59
[42] Johnson G C and Lyman J M 2020 Warming trends increasingly dominate global ocean *Nat. Clim. Change* **10** 757–61
[43] Cornec M, Claustre H, Mignot A, Guidi L, Lacour L, Poteau A, D'Ortenzio F, Gentili B and Schmechtig C 2021 Deep chlorophyll maxima in the global ocean: occurrences, drivers and characteristics *Glob. Biogeochem. Cycle* **35** e2020GB006759
[44] Quartly G D, Aiken J, Brewin R J W and Yool A 2023 The link between surface and sub-surface chlorophyll-a in the centre of the Atlantic subtropical gyres: a comparison of observations and models *Front. Mar. Sci.* **10** 1197753
[45] AVISO 2019 SSALTO/DUACS user handbook: (M)SLA and (M)ADT near-real time and delayed time products (AVISO Publ) CLS-DOS-NT-06-034, SALP-MU-PEA-21065-CLS
[46] Quartly G D *et al* 2017 A new phase in the production of quality-controlled sea level data *Earth Syst. Sci. Data* **9** 557–72
[47] Tian F L, Wu D, Yuan L M and Chen G 2020 Impacts of the efficiencies of identification and tracking algorithms on the statistical properties of global mesoscale eddies using merged altimeter data *Int. J. Remote Sens.* **41** 2835–60
[48] Chelton D B, Schlax M G and Samelson R M 2011 Global observations of nonlinear mesoscale eddies *Prog. Oceanogr.* **91** 167–216
[49] Chen G and Han G Y 2019 Contrasting short-lived with long-lived mesoscale eddies in the global ocean *J. Geophys. Res.: Oceans* **124** 3149–67
[50] Sathyendranath S, Jackson T, Brockmann C, Brotas V, Calton B and Chuprin A 2020 *ESA Ocean Colour Climate Change Initiative (Ocean_Colour_CCI): Global Chlorophyll-a Data Products Gridded on a Sinusoidal Projection, Version 4.2* (Centre for Environmental Data Analysis)
[51] Campbell J W 1995 The lognormal distribution as a model for bio-optical variability in the sea *J. Geophys. Res.: Oceans* **100** 13237–54
[52] He Q Y, Zhan H G, Xu J, Cai S Q, Zhan W K, Zhou L B and Zha G Z 2019 Eddy-induced chlorophyll anomalies in the western South China Sea *J. Geophys. Res.: Oceans* **124** 9487–506
[53] Holte J, Talley L D, Gilson J and Roemmich D 2017 An Argo mixed layer climatology and database *Geophys. Res. Lett.* **44** 5618–26
[54] Rohr T, Harrison C, Long M C, Gaube P and Doney S C 2020 The simulated biological response to Southern Ocean eddies via biological rate modification and physical transport *Glob. Biogeochem. Cycle* **34** e2019GB006385
[55] Liu Q, Liu Y J and Li X F 2023 Characteristics of surface physical and biogeochemical parameters within mesoscale eddies in the Southern Ocean *Biogeosciences* **20** 4857–74
[56] NOAA Physical Sciences Laboratory 2021 NOAA OI SST V2 High Resolution Dataset
[57] Wong A P S 2020 Argo data 1999–2019: Two million temperature-salinity profiles and subsurface velocity observations from a global array of profiling floats *Front. Mar. Sci.* **7** 700